

FEDSM-ICNMM2010-31209

FLOW PATTERNS AND CHF IN A LOCALLY HEATED LIQUID FILM SHEAR-DRIVEN IN A MINICHANNEL

Zaitsev D.V.^{1,2} and Kabov O.A.^{1,2}

1- Institute of Thermophysics SB RAS, Novosibirsk, Russia, Email: zaitsev@itp.nsc.ru

2- Universite Libre de Bruxelles, Microgravity Research Center, Bruxelles, Belgium, Email: okabov@ulb.ac.be

ABSTRACT

Thin and very thin (less than 10 μm) liquid films driven by a forced gas/vapor flow (stratified or annular flows), i.e. shear-driven liquid films in a narrow channel is a promising candidate for the thermal management of advanced semiconductor devices in earth and space applications. Development of such technology requires significant advances in fundamental research, since the stability of joint flow of locally heated liquid film and gas is a rather complex problem. The paper focuses on the recent progress that has been achieved by the authors through conducting experiments. Experiments with water in flat channels with height of $H=1.2\text{-}2.0$ mm (mini-scale) show that a liquid film driven by the action of a gas flow is stable in a wide range of liquid/gas flow rates. Map of isothermal flow regime was plotted and the length of smooth region was measured. Even for sufficiently high gas flow rates an important thermocapillary effect on film dynamics occurs. Scenario of film rupture differs widely for different flow regimes. It is found that the critical heat flux for a shear driven film can be 10 times higher than that for a falling liquid film, and exceeds 400 W/cm^2 in experiments with water for moderate liquid flow rates. This fact makes use of shear-driven liquid films promising in high heat flux chip cooling applications.

INTRODUCTION

The fast development in semiconductor technology, including shrinking feature size, increasing transistor density, and faster circuit speeds, is leading to ever higher chip power dissipation and heat fluxes. Moreover, increasing performance demands have resulted in greater non-uniformity of on-chip power dissipation, creating localized, sub-millimeter hot spots, often exceeding $1\text{ kW}/\text{cm}^2$ in heat flux, which can degrade the processor performance and reliability [1,2,3]. Thin and very thin (less than 10 μm) liquid film driven by a forced gas/vapor flow (annular flows [3, 4] or stratified flows [5,6,7]), i.e. shear-driven liquid film in a narrow channel (100-500 μm [8]) is a

promising candidate for the thermal management of advanced semiconductor devices in terrestrial and space applications.

Development of such technology requires significant advances in fundamental research, since the stability of joint flow of locally heated liquid film and gas is a rather complex problem [9,10,11,12]. Moreover, studies of such liquid films require precision measurements and accurate models of the transition regimes between macro and micro-scale, which are capable to predict formation of dry patches and heat transfer in the micro-region near contact line and hence in the localized hot spots with intensive evaporation. The film deformations, formation of dry patches as well as heat transfer are governed by viscous, capillary, inertial, and contact-line forces [13, 14]. It is shown in [15] that the heat flux density of an evaporating thin liquid film may reach a local maximum of 1800 W/cm^2 near the contact line area of the fluid on the heated wall.

The disruption of liquid films on a heated wall is of major technical importance since it determines the allowed heat transfer rate in a number of engineering applications. Motivated by potential application of liquid films in cooling of microelectronics recent studies of the authors of the present paper [16,17,18,19] have been focused on subcooled thin liquid films falling down a locally heated plate. In the experiments the occurrence of novel instabilities forming a rivulet structure wavelike in spanwise direction (“regular structures”) was revealed. It was found also that on local heaters with length of several millimeters the film rupture occurs at heat fluxes of about one order of magnitude higher than on heaters with length of around 1 m [16]. However, the critical heat flux (CHF) for a locally heated falling liquid film is still limited by several tens of W/cm^2 for water; for FC-72 the CHF is even lower [8, 16]. These CHF values are not sufficient for the modern powerful microelectronics.

Rupture of a horizontal liquid layer non-uniformly heated from below is investigated in [20,21]. In 0.85–1.3 mm thick layers of ethanol [20] the appearance of a dry patch is preceded by formation of a thinned region in the film with convective

cells pattern. At the threshold heat flux a dry patch quickly originates as a pinhole within the thinned region. In 0.13–1.68 mm thick silicon-oil layers [21] the heating causes a steady state thermocapillary dimple above the heater, gradually deepening with the heat flux, until finally the edge of the dimple touches the substrate, with formation of a nearly dry patch, remaining covered with a thin layer of oil less than 1 μm thick. In our work [22] rupture of a subcooled locally heated liquid film flowing over horizontal and slightly inclined plates have been studied, which, in a sense, fills the gap between studies [16,17] and [20,21].

Contrary to gravity-driven liquid films, shear-driven films are less likely to rupture [7], this provides a way to prevent and control a hot dry patch formation by the shear stress induced by gas flow. It is quite evident that the combined effects of evaporation, thermocapillarity, gas dynamics, and gravity as well as the formation of microscopic adsorbed film on the wall, are somewhat complicated issues and have not yet been studied systematically. The aim of the present work is to give an overview of the recent progress that has been achieved by the authors through conducting experiments with locally heated liquid films moving under the friction of a forced gas flow in a mini-channel. The design of the heater used in [7] did not allow to achieve heat fluxes higher than 30 W/cm^2 . In the present work we use a new test section specially designed for achieving high heat fluxes (up to 500 W/cm^2).

NOMENCLATURE

- c_p thermal capacity, J/kgK
- H channel height, mm
- g gravitational acceleration, m/s^2
- h film thickness, m
- L_{sm} length of region of smooth film, mm
- q heat flux density, W/m^2
- q_{idp} threshold heat flux at which an initial stable dry patch forms, W/m^2
- $q_{idp,H}$ threshold heat flux at which an initial stable dry patch forms on the heater, W/m^2
- Re Reynolds number $=\Gamma\rho/\mu$, dimensionless
- T temperature, $^\circ\text{C}$
- U_s superficial velocity $=\Gamma/H$, m/s

Greek symbols

- Γ specific volumetric flow rate, m^2/s
- ρ density, kg/m^3
- μ dynamic viscosity, $\text{kg}/\text{m s}$
- σ surface tension coefficient, N/m

Subscripts

- 0 initial parameters of the flow
- g, l gas and liquid
- W wall (heater)

1. EXPERIMENTAL SETUP

Schematic of experimental setup is presented in Fig. 1. Figure 2 shows design of the test section. The main part of the test section is a thin stainless steel plate with a flush-mounted copper rod. At the working surface the rod has a 1×1 cm square head emulating surface of a computer chip (Fig. 2). The rod is heated by a heating spiral coiled around its bottom part. Such

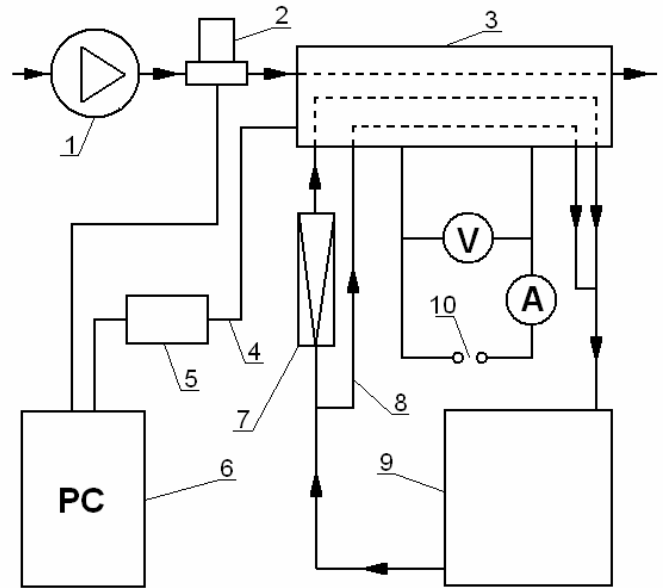


Fig. 1. Schematic of experimental setup. 1- gas compressor; 2- gas flow meter; 3- test section; 4- signal from thermocouples; 5- amplifier and analog-to-digital converter; 6- personal computer; 7- liquid rotameter; 8- line to thermostabilizer; 9- thermostatic bath; 10- DC power supply.

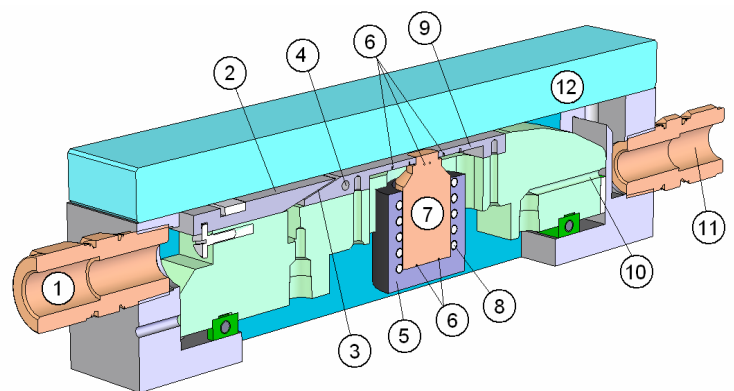


Fig. 2. Design of test section. 1- gas inlet; 2- channel; 3- liquid nozzle; 4- thermocouple; 5- heat insulation; 6- thermocouples; 7- copper rod; 8- Nichrome spiral; 9- stainless steel plate; 10- liquid outlet; 11- gas outlet; 12 – glass cover.

construction of the heater provides the condition at the heater surface $T=\text{const}$ (which is confirmed by thermocouples measurements). The test section is covered with a transparent cover made of optical glass so that a flat channel is formed. We applied three different channel heights, namely: 1.2, 1.5 and 2 mm. Gas, pumped by a compressor, flows through the channel and passes to the atmosphere at the end of the test section. Gas flow rate is measured by a Bronkhorst digital thermal mass flow meter with an accuracy of 1%. Liquid, supplied from a thermostat, gets into the channel through a liquid nozzle and flows under the friction of the gas along the stainless steel plate as a film. The liquid is accumulating at the bottom part of the test section and is returned into the thermostat. The liquid flow rate is measured by a float-type rotameter with an accuracy of 1.5%. The stainless steel plate is kept at constant temperature by a 3 mm diameter channel through which the working liquid is pumped (see 8 in Fig.1 and 4 in Fig. 2).

Distance from the gas inlet to the liquid nozzle is 57 mm while distance from the liquid nozzle to the heater is 32 mm. This provides steady flows of gas and liquid at the moment they reach the heater. Channel width is 30 mm. Several thermocouples are embedded in the stainless steel plate and in the copper rod, as depicted in Fig.2, allowing determination of the working surface temperature. The temperature of the heater surface is calculated taking into account the depth at which the thermocouples are embedded (2 mm). All the thermocouples are individually calibrated to an accuracy of 0.1°C.

The heat flux is determined by the electrical power dissipated on the heating spiral. Thermal conductivity of copper is 400 W/mK which is almost 30 times higher than that of stainless steel (15 W/mK). This provides heat spreading from the heater to the stainless steel plate of about 10% at $q>250$ W/cm², of about 20% at $q=100$ W/cm² and of up to 30% for smaller heat fluxes (according to the measurements by thermocouples embedded into the substrate). In order to minimize heat spreading from the heating spiral into the atmosphere, the heating spiral is wrapped with a layer of heat insulation material (mineral wool).

Distilled water with initial temperature of 24°C is used as the working liquid. Air with temperature of 24-27 °C and relative humidity of 15-30% is used as the working gas. Atmospheric pressure during experiments varied from 98500 to 101600 Pa. The experiments are carried under stationary conditions. Superficial gas velocity (volumetric gas flow rate divided by cross-sectional area of the channel) U_{sg} varies from 0.1 to 34 m/s. Maximum pressure drop along the channel takes place at maximum gas flow rate and is estimated to be less than 500 Pa. The test section is set horizontally. When investigating liquid films falling under the action of gravity the test section is set vertically while the glass cover is removed.

2. ISOTHERMAL FLOW

Isothermal flow (heater switched off) was investigated at $H=1.5$ mm in the ranges of $Re_l=5-180$ and $Re_g=10-2550$ ($U_{sg}=0.1-26.5$ m/s). The maximum values of these ranges were limited by pumping power of liquid pump and gas compressor.

Figure 3 shows the flow regime map obtained. Figure 4 presents photographs of typical regimes. At sufficiently small Re_l the film ruptures, Fig. 3, Fig. 4d. At sufficiently small Re_g channel flooding occurs, Fig. 3. Here we define the channel flooding as when the width of the gas flow in the area of the heater is reduced by at least 10%, Fig. 4c. Figure 3 presents also domains of smooth film in the area of the heater, 2D waves occurrence in the area of the heater (Fig. 4b) and 3D waves occurrence in the area of the heater (Fig. 4a). The map presented in Fig. 3 qualitatively agrees with that obtained in [7], however from quantitative point of view there is a wide discrepancy. The reason is that characteristics of the test section used in [7] – such as distance from the liquid nozzle to the heater, flow width, channel height, substrate wettability properties – are different from those in the present study.

Figure 5 presents influence of Re_l and U_{sg} on the length from the liquid nozzle to the beginning of the wave formation, i.e. the length of smooth region, L_{sm} . Statistical error in determining L_{sm} is about ± 3 mm. In general, L_{sm} decreases with increasing U_{sg} and with decreasing Re_l . However for $6 \leq Re_l \leq 36$ and $120 \leq Re_l \leq 180$ L_{sm} is practically independent on Re_l (within the limits of experimental error). This is consistent with [7] where Re_l was found to have little or no effect on L_{sm} in the range $9 \leq Re_l \leq 29$. As it is seen from Fig. 5, data on L_{sm} from [7] correlates well with the present data.

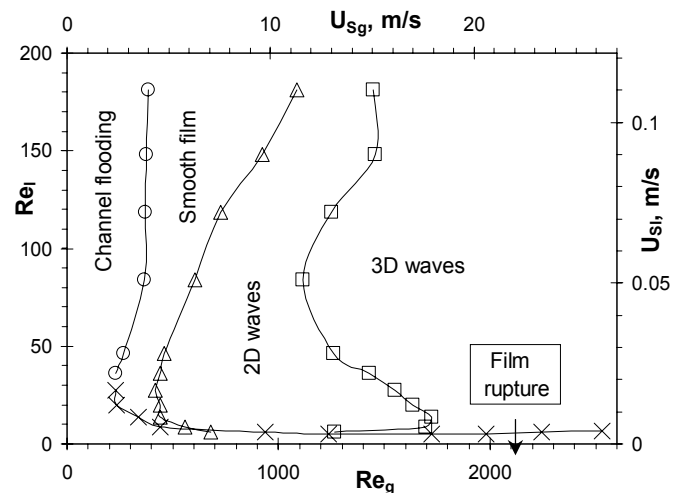


Fig. 3. Map of isothermal flow regimes, $H=1.5$ mm.

3. FILM RUPTURE AND CHF UNDER LOCAL HEATING

Disruption of the liquid film under local heating was investigated at $H=1.2, 1.5$ and 2 mm, in the ranges of $q=0-410$ W/cm², $Re_l=8.5-84$, $Re_g=350-2600$, $U_{sg}=3.8-34$ m/s. Figure 6 illustrates the process of film disruption with increase of the heat flux at $H=1.2$ mm, $Re_l=30$, $Re_g=2550$ ($U_{sg}=30$ m/s). At a certain threshold heat flux q_{idp} the film ruptures with formation of a dry patch on the substrate. As usual, first dry patches initiate downstream of the heater along its lateral edges, as

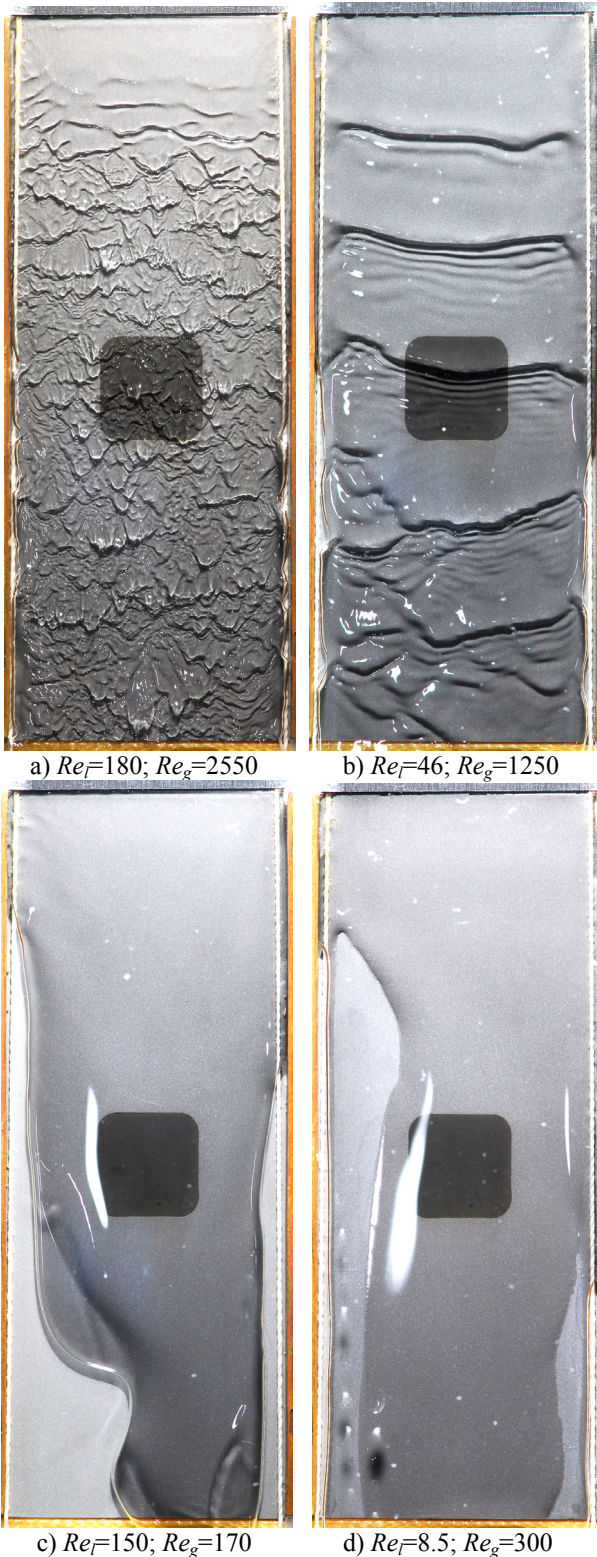


Fig. 4. Photographs of 3D waves (a), 2D waves (b), channel flooding (c) and film rupture (d). Isothermal flow, $H=1.5$ mm. Flow directed from top to bottom.

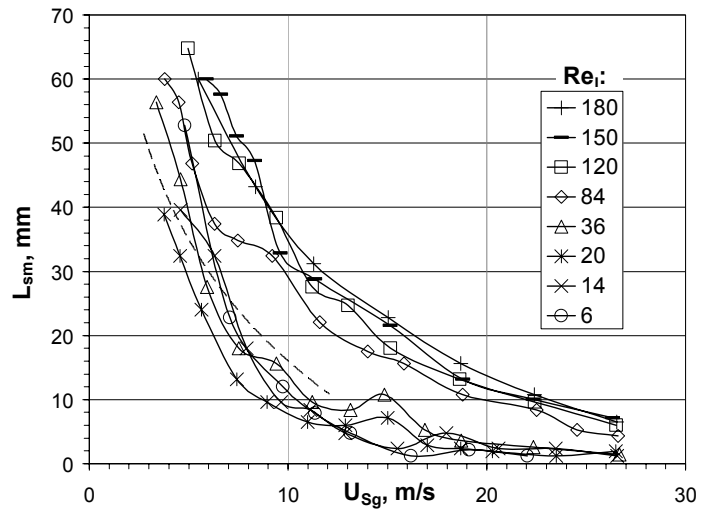


Fig. 5. Length of smooth region in the film, depending on superficial velocity of gas for different Reynolds numbers of liquid, $H=1.5$ mm. Dashed curve – generalization of data [7] for $Re_l=9-29$, $H=2$ mm.

depicted in Fig. 6a. In the present study we deal with thermocapillary film rupture, since dry patches initiate at temperatures well below the saturation temperature, Fig. 6a. Thermocapillary tangential stresses at the film surface, induced by the dependence of the liquid surface tension on the temperature, and tangential stresses, induced by the flowing gas, are the main competitive forces. The film is thinnest along the lateral edges of the heater where temperature gradient at the film surface attains its maximum values. Film rupture is most likely to occur in this area.

At a slightly higher heat flux $q_{idp,H}$ dry patches reach the heater, Fig. 6b (for smaller Re_g and smaller Re_l $q_{idp,H}=q_{idp}$). With further increase of the heat flux, virtually entire heater is covered with metastable, intensively evaporating thin liquid film, with quickly emerging and disappearing small dry patches, Fig. 6c-e. And finally at the critical heat flux q_{cr} , the heater is suddenly dried out and its temperature starts to rise rapidly, Fig. 6f.

Figure 7 shows the effect of superficial gas velocity on the threshold heat flux for film rupture and on CHF, at $Re_l=14$. For comparison, data for falling liquid film is also presented (at $Re_l=14$ $q_{idp}=q_{idp,H}=q_{cr}$). It is seen that at relatively small U_{sg} , $q_{idp,H}$ and q_{cr} for shear-driven liquid film are close to those for falling liquid film. However at higher gas velocities, $q_{idp,H}$ for shear-driven liquid film is up to 3 times higher, while q_{cr} , almost linearly growing with U_{sg} , at $U_{sg}=34$ m/s is more than 10 times higher and reaches 250 W/cm². For shear-driven liquid film with an increase of gas velocity inertial force starts to dominate acting against thermocapillary forces, which provides more uniform liquid distribution over the heater as compared to gravity-driven liquid film. As a result, q_{cr} can be several times higher than q_{idp} and $q_{idp,H}$.

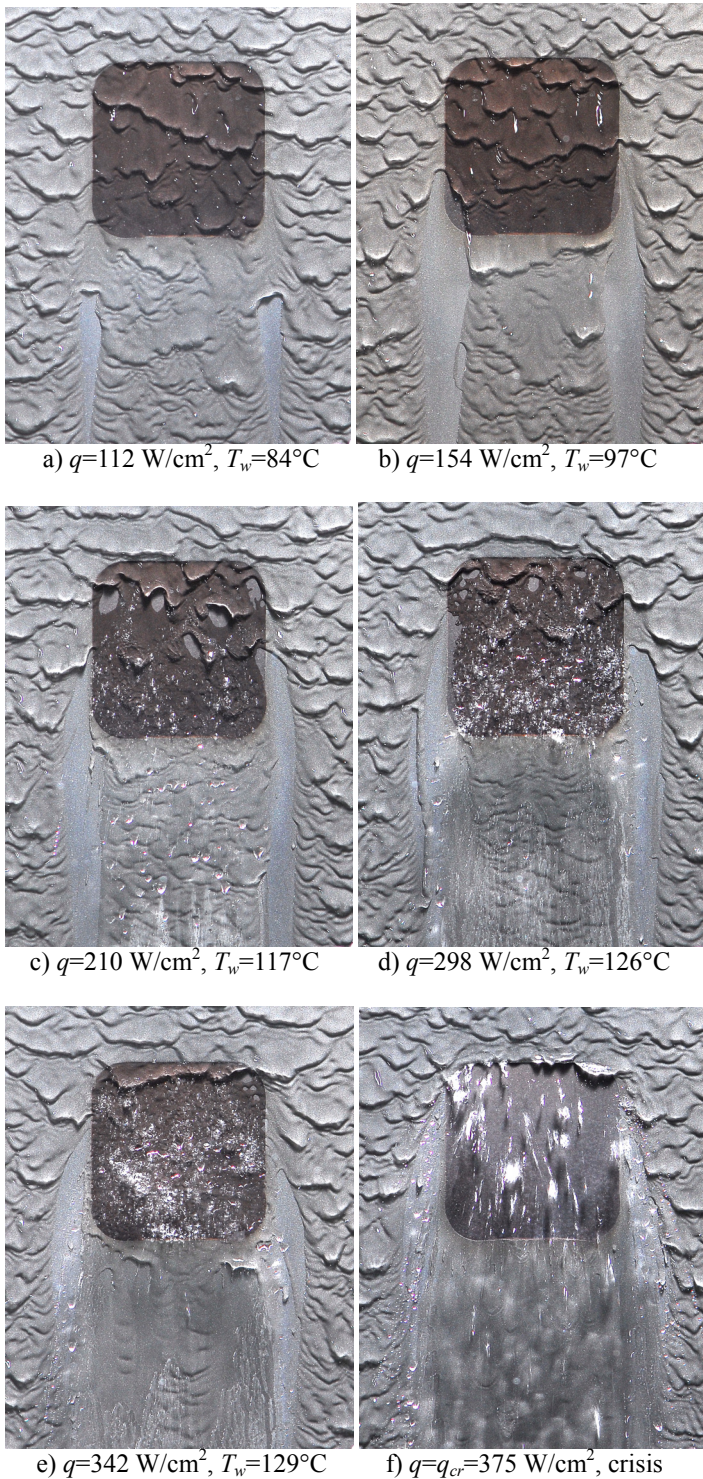


Fig. 6. Film rupture and crisis in shear-driven liquid film, $H=1.2$ mm, $Re_f=30$, $Re_g=2550$ ($U_{sg}=30$ m/s), flow directed from top to bottom.

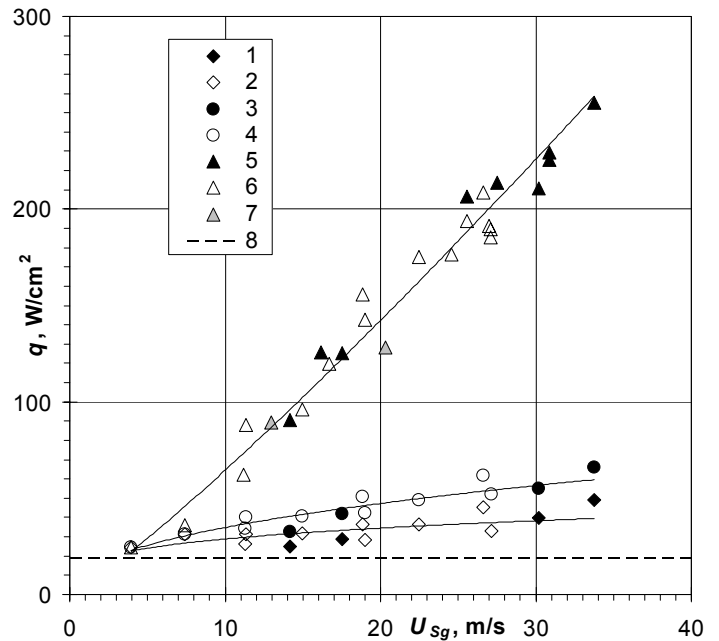


Fig. 7. Effect of superficial gas velocity on film rupture and CHF, $Re_f=14$. 1- q_{idp} at $H=1.2$ mm; 2- q_{idp} at $H=1.5$ mm; 3- $q_{idp,H}$ at $H=1.2$ mm; 4- $q_{idp,H}$ at $H=1.5$ mm; 5- q_{cr} at $H=1.2$ mm; 6- q_{cr} at $H=1.5$ mm; 7- q_{cr} at $H=2$ mm; 8- $q_{idp}=q_{idp,H}=q_{cr}$ for a falling liquid film, Fig. 8. Curves, generalizing data for q_{idp} , $q_{idp,H}$ and q_{cr} are plotted.

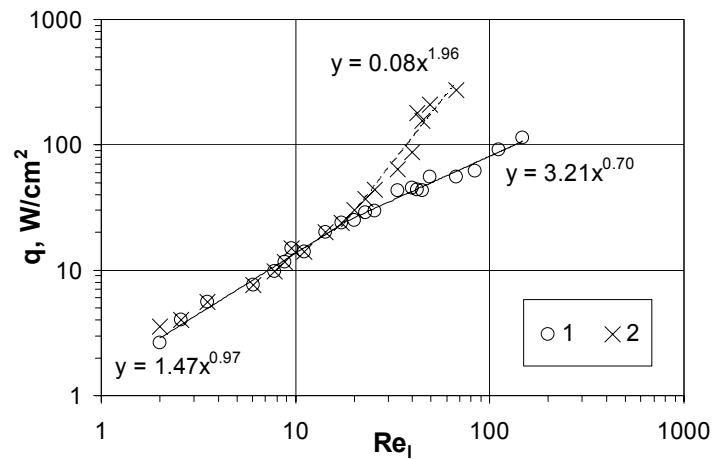


Fig. 8. Data on $q_{idp}=q_{idp,H}$ (1) and q_{cr} (2) for falling liquid film (test section in vertical orientation with no gas flow and with glass cover removed). Generalization curves and corresponding equations are shown.

More data obtained for falling liquid film is presented in Fig. 8. For gravity-driven films the first stable dry patch always forms on the heater, i.e. $q_{idp}=q_{idp,H}$. Moreover, for $Re_l < 20$ $q_{idp}=q_{idp,H}=q_{cr}$, which means that the first dry patch inevitably spreads all over the heater and results in crisis occurrence. For

$Re_f \geq 20$ $q_{cr} > q_{idp} = q_{idp,H}$, with q_{cr} quickly rising with respect to $q_{idp} = q_{idp,H}$ as Re_f is increased. We attribute this phenomenon to the effect of boundaries of the film flow. The width of the flow is relatively small (30 mm) and for higher film thicknesses the boundaries of the film begin to affect the film in the area of the heater, in particular, forming a rivulet on the heater and thus preventing dry patches from spreading all over the heater, Fig. 9. For falling liquid film at $Re_f \geq 20$ and $q > q_{idp} = q_{idp,H}$ an essential part of the heater is dry, Fig. 9. The heater temperature is stable because of boiling in the film, still covering minor part of the heater.

In case of shear-driven liquid film, the film thickness is much smaller and the boundaries practically do not affect the film near the heater (this is seen from Fig. 6: upstream the heater 3D wave structure is uniform in spanwise direction).

Figure 10 shows the effect of gas velocity on CHF for a shear-driven liquid film for different Re_f and different H . It is seen that CHF grows with increase of both U_{Sg} and Re_f . Unfortunately, the power supply did not allow to achieve heat flux higher than 410 W/cm^2 (point $Re_f=46$, $H=1.2 \text{ mm}$, $U_{Sg}=26 \text{ m/s}$).

From Figs. 7 and 10 it is seen that the channel height has no or little effect on q_{cr} (within the ranges studied and within the limits of experimental error).

4. EFFECT OF INCLINATION ANGLE

Figure 11 presents data on q_{cr} for different inclination angles of the test section with respect to the horizon, Θ , for $Re_f=14$, $H=1.5 \text{ mm}$. In the experiment Θ varied with a step of 45° from 0 to 360° . It is seen that CHF is weakly affected by the inclination angle, except in the case of $\Theta=-90^\circ$, where two points falls out of the generalization. This is due to the fact that at $\Theta=-90^\circ$ for smaller Re_g the heater is periodically washed by the liquid, which prevents the occurrence of the heat transfer crisis.

The map of isothermal flow regimes for $\Theta=-90^\circ$, $H=1.5 \text{ mm}$ is presented in Fig. 12. It is seen, in comparison with $\Theta=0$, $H=1.5 \text{ mm}$ (Fig. 3), that there is no regimes with “2D waves” and “smooth film”, while the area of “channel flooding” is considerably wider.

5. DISCUSSION AND CONCLUSIONS

The high heat fluxes achieved makes use of shear-driven liquid films promising in cooling applications. Since the experiment was performed at atmospheric pressure, sufficiently high wall temperatures take place (up to $T_w=130^\circ\text{C}$ prior to crisis, see Fig. 6). High temperature is needed to ensure intensive evaporation. It is evident that decrease of the pressure in the system will allow to decrease the heater temperature, what is needed for microelectronics cooling. Further investigations with lower pressures are necessary.

From practical point of view, it is worth noting that the pumping power in a cooling system, based on shear-driven

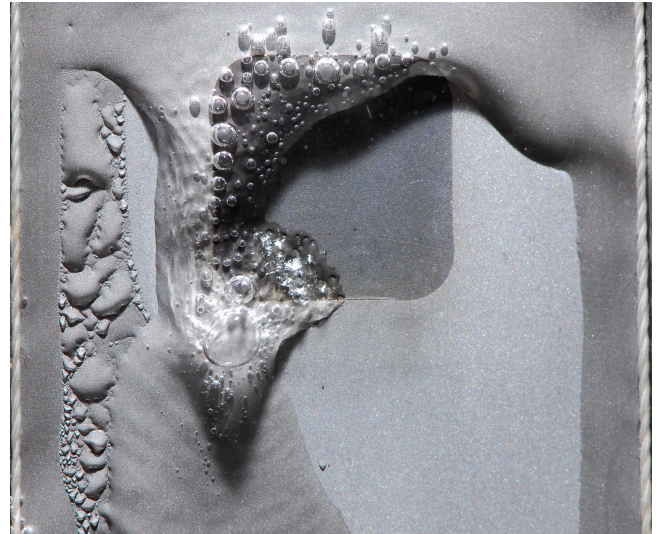


Fig. 9. Rupture of falling liquid film, $Re_f=46$, $q=100 \text{ W/cm}^2$ ($q_{cr}=160 \text{ W/cm}^2$). Flow directed from top to bottom.

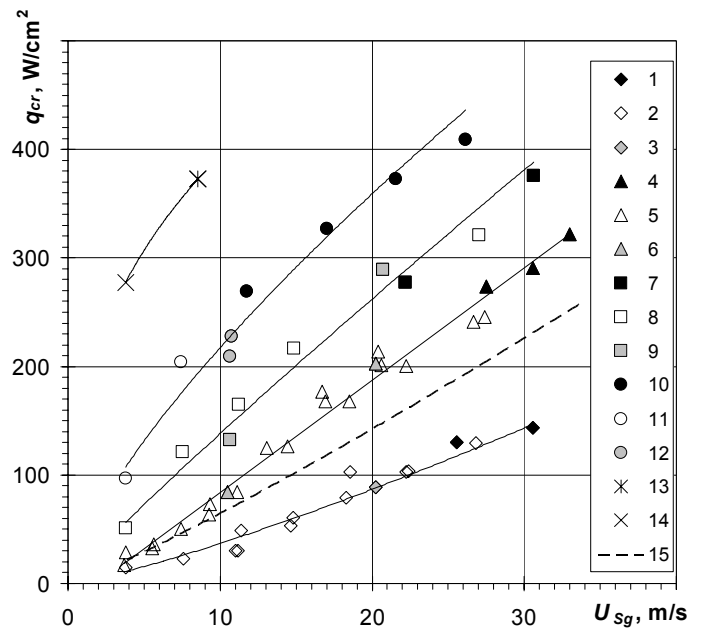


Fig. 10. Effect of gas velocity on CHF for different liquid flow rates and different channel heights. 1- $Re_f=8.5$, $H=1.2 \text{ mm}$; 2- $Re_f=8.5$, $H=1.5 \text{ mm}$; 3- $Re_f=8.5$, $H=2 \text{ mm}$; 4- $Re_f=20$, $H=1.2 \text{ mm}$; 5- $Re_f=20$, $H=1.5 \text{ mm}$; 6- $Re_f=20$, $H=2 \text{ mm}$; 7- $Re_f=30$, $H=1.2 \text{ mm}$; 8- $Re_f=30$, $H=1.5 \text{ mm}$; 9- $Re_f=30$, $H=2 \text{ mm}$; 10- $Re_f=46$, $H=1.2 \text{ mm}$; 11- $Re_f=46$, $H=1.5 \text{ mm}$; 12- $Re_f=46$, $H=2 \text{ mm}$; 13- $Re_f=84$, $H=1.2 \text{ mm}$; 14- $Re_f=84$, $H=1.5 \text{ mm}$; 15- generalization of data for $Re_f=14$, $H=1.2-2 \text{ mm}$, Fig. 7. Curves, generalizing data are plotted for each Re_f .

liquid film, is much higher than that in a cooling system, based on falling liquid film. Pumping power is directly related to the operating cost of a cooling system [23-24]. Comparison of the CHF between these two systems under a fixed pumping power is necessary.

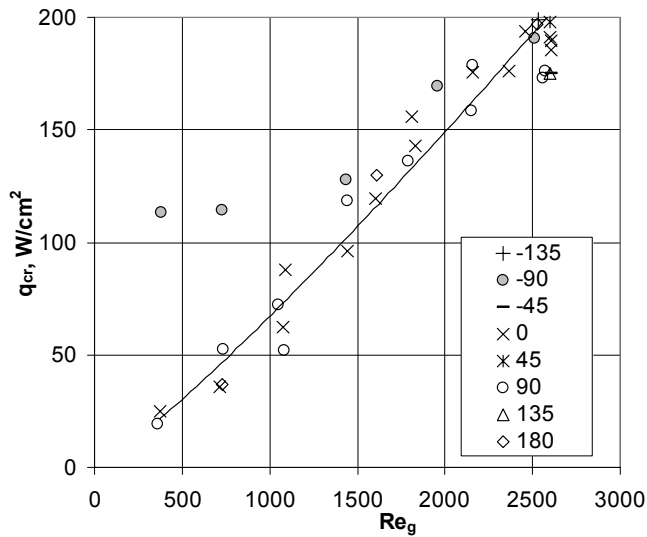


Fig. 11. CHF for different inclination angles of the test section with respect to the horizon, θ (indicated in legend), for $Re_l=14$, $H=1.5$ mm.

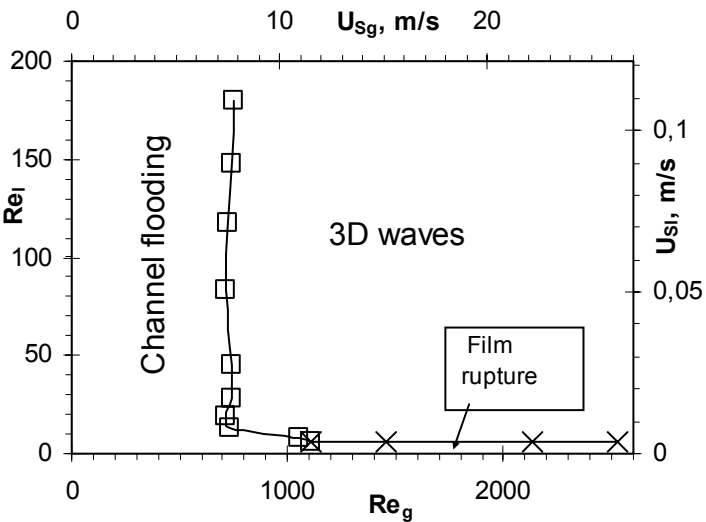


Fig. 12. Map of isothermal flow regimes, $\theta=-90^\circ$, $H=1.5$ mm.

ACKNOWLEDGMENTS

The authors gratefully acknowledge support of this work by CRDF (RUE1-2846-NO-06), ONR NICOP Grant N00014-08-1-0263 and SAFIR PRODEX Programme (Belgium).

REFERENCES

- [1] Wang P., Bar-Cohen A., Yang B., Solbreken G.L., Zhang Y. and Shakouri A., "Thermoelectric Micro-Cooler for Hot-Spot Thermal Management", Proc. InterPACK'05: Tech. Conf. and Exhibition on Integration and Packaging of MEMS, NMES and Electronic Systems, San Francisco, paper IPACK2005-73244, 2005.
- [2] Mahajan R., Chiu C., Chrysler G., "Cooling a Microprocessor Chip", Proceedings of the IEEE, 94, 8, 1476-1486, 2006.
- [3] Bar-Cohen A. and Rahim E., "Modeling and prediction of two-phase refrigerant flow regimes and heat transfer characteristics in microap channels", Proceedings of the 5th International Conference on Nanochannels, Microchannels and Minichannels, June 18-20, 2007, Puebla, Mexico, 2007.
- [4] Bar-Cohen A., Sherwood G., Hodes M., and Solbreken G., "Gas-Assisted Evaporative Cooling of High Density Electronic Modules", IEEE Transactions on Components, Hybrids, and Manufacturing Technology, 18, 3, 502-509, 1995.
- [5] Kabov O.A., Kuznetsov V.V. and Legros J-C., "Heat transfer and film dynamic in shear-driven liquid film cooling system of microelectronic equipment", Proc. II Int. Conf. on Microchannels and Minichannels, Rochester, pp. 687-694, 2004.
- [6] Gatapova E.Ya., Kabov O.A., Marchuk I.V., "Thermocapillary deformation of a locally heated liquid film moving under the action of a gas flow". Tech. Phys. Lett., 30, 5, 418-421, 2004.
- [7] Kabov O.A., Lyulin Yu.V., Marchuk I.V. and Zaitsev D.V. "Locally heated shear-driven liquid films in microchannels and minichannels", International Journal of Heat and Fluid Flow, Vol. 28, pp. 103-112, 2007.
- [8] Kabov O., "Cooling of Microelectronics by Thin Liquid Films", Keynote lecture, Proc. Int. Workshop on "Wave Dynamics and Stability of Thin Film Flow Systems", September 1-4, Chennai, India, Narosa Publishing House, 279-311, 2006.
- [9] Hewitt G.F. and Hall-Taylor M.S., "Annular two-phase flow", Pergamon Press, Oxford, 1970.
- [10] Hanratty T.J., "Separated flow modeling and interfacial transport phenomena", Appl. Sci. Res., vol. 48, pp. 353-390, 1991.
- [11] Aktershev S.P., and Alekseenko S.V., "Interfacial Instabilities in an Annular Two-Phase Flow", Russ. J. Eng. Thermophys, vol. 6(4), pp. 307-320, 1996.
- [12] H. Roskamp, M. Willmann and S. Wittig, "Heat up and evaporation of shear driven liquid wall films in hot turbulent air flow", Int. J. Heat and Fluid Flow, vol. 19, pp. 167-172, 1998.

- [13] M. Potash and P.C. Wayner, "Evaporation from a two-dimensional extended meniscus", *Int. J. Heat Mass Transfer*, vol. 15, pp. 1851-1863, 1972.
- [14] V.S. Ajaev, "Spreading of thin volatile liquid droplets on uniformly heated surfaces", *J. Fluid Mech.*, vol. 528, pp. 279-296, 2005.
- [15] Stephan P. and Brandt C., "Advanced capillary structures for high performance heat pipes", *Proc. I Int. Conf. on Microchannels and Minichannels*, Ed. S.G. Kandlikar, April 24-25, 2003, Rochester, NY, pp. 69-75, 2003.
- [16] Kabov O.A., "Breakdown of a liquid film flowing over the surface with a local heat source", *Thermophysics and Aeromechanics*, 7, 4, 513-520, 2000.
- [17] Chinnov E.A., Kabov O.A., Muzykantov A.V., Zaitsev D.V., "Influence of plate inclination on heat transfer and breakdown of locally heated flowing liquid film", *Intern. Journal of Heat and Technology*, 19, 1, 31-44, 2001.
- [18] Kabov O.A., Benoit S., Sharina I.A., Legros J.-C., "Heat transfer and rivulet structures formation in a falling thin liquid film locally heated", *Int. J. Therm. Sci.*, 41, 664-672, 2002.
- [19] Frank A.M., Kabov O.A., "Thermocapillary structure formation in a falling film: experiment and calculations", *Phys. Fluids*, 18, 032107-1 - 032107-10, 2006.
- [20] Orell A., Bankoff S. G., "Formation of a Dry Spot in a Horizontal Liquid Film Heated from Below," *Int. J. Heat and Mass Transfer*, 14, 1835-1842, 1971.
- [21] Burelbach J. P., Bankoff S. G., Davis S. H., "Steady thermocapillary flows of thin liquid layers. II. Experiment", *Phys. Fluids A* 2, 321-333, 1990.
- [22] D.V. Zaitsev, O.A. Kabov, "An experimental modeling of gravity effect on rupture of a locally heated liquid film", *Microgravity sci. technol.*, XIX-3/4, p. 174-177, 2007.
- [23] P. Wildi-Tremblay, L. Gosselin, "Minimizing shell-and-tube heat exchanger cost with genetic algorithms and considering maintenance", *Int. J. Energy Res.* 31 867-885, 2007.
- [24] S.J. Kim, D.K. Kim, H.H. Oh, "Comparison of fluid flow and thermal characteristics of plate-fin and pin-fin heat sinks subject to a parallel flow", *Heat Transfer Engineering* 29(2), 169-177, 2008.